

A discrete strong embedded discontinuity approach

J. Alfaiate

Instituto Superior Técnico and ICIST, Dept. Eng. Civil, Lisboa, Portugal

L. J. Sluys

Delft University of Technology, Dept. of Civil Eng. and Geosciences, Delft, The Netherlands

ABSTRACT: In this paper, a new formulation for strong embedded discontinuities is introduced, designated as the *discrete strong embedded discontinuity approach (DSDA)*. The approximated displacement field is discontinuous across the embedded discontinuity and the jumps are obtained at additional nodes, located at both faces of the discontinuity surface. As a consequence: i) the jump displacement field no longer has to be homogeneous within each element and ii) the jump displacement field is continuous across element boundaries. The present formulation is compared with other discontinuous approaches, namely the discrete approach with interface elements, the partition of unity method and other strong embedded discontinuity formulations.

Keywords: strong embedded discontinuity, discrete cracking

1 INTRODUCTION

Two major classes of finite element models have been used in the past to describe fracture in concrete: the continuum models and the discontinuous models. In the former case, cracking is smeared over a band or an element and the material constitutive relation is modified to take strain softening into account. In the second case, cracking is assumed to localize in a discrete surface with initial zero width. As a consequence, the material no longer remains continuous after crack initiation.

More recently, embedded discontinuities in finite elements were introduced, giving rise to weak embedded discontinuity formulations (Sluys 1998) and strong embedded discontinuity formulations (*SED*) (Simo et al. 1993). The former models are still representative of a continuum approach, whereas the strong discontinuity, which represents the limit case of a weak discontinuity when the width of the band tends to zero, is a discrete concept. In Oliver et al. (2002), a model is introduced which takes into account the transition between weak and strong dis-

continuities. In this work, the discrete constitutive relation is obtained as the projection of the continuum behavior at the discontinuity surface. This formulation is called the *continuum strong discontinuity approach (CSDA)* since the complete behavior is derived from the continuum (Samaniego 2003). In this formulation, the displacement jumps are constant within each parent finite element; as a result, the jumps are not continuous across the element boundaries.

Another formulation which takes into account the transition between weak and strong discontinuities can be found in Simone et al. (2003). In this work, an enhanced gradient damage model is used first to model the behaviour of the continuum. Next, when a certain degree of damage is attained in the material, a strong discontinuity approach is adopted by means of the partition of unity model (*PUM*) (Wells and Sluys 2001a). In this case, the jumps are continuous across the boundaries of the parent elements, but the concept of embedded discontinuities is no longer addressed.

In this paper a *discrete strong embedded discontinuity approach (DSDA)* is proposed as an alternative to previous strong embedded discontinuity formulations. When cracking initiates, the material unloads in the neighboring area in order to fulfill equilibrium, i.e., the traction continuity condition. Assuming that the bulk remains elastic, all nonlinear mechanical properties are prescribed at the discrete or localized level: i) a crack initiation criterion can be obtained from a limit surface in the traction space (Alfaiate and Sluys 2002) and ii) a discrete constitutive relation can be explicitly introduced for the discontinuity. Furthermore, since no continuum-discontinuous transition is assumed, the approximated displacement field is discontinuous, similar to the discrete-interface approach: the approximated displacement jumps are obtained at additional nodes, located at both faces of the discontinuity surface. In this formulation, non-homogeneous jump displacement fields are obtained within each parent element and the jumps are continuous across element boundaries. The *DSDA* is compared with other discontinuous formulations, namely the discrete-interface approach and the *PUM* (Wells and Sluys 2001a), as well as with a previous embedded discontinuity formulation introduced in Alfaiate et al. (2003b).

2 KINEMATICS OF A DISCONTINUITY

Consider a domain Ω , with boundary $\partial\Omega$, where a discontinuity surface Γ_d is supposed to exist (fig.1). In Alfaiate et al. (2003b), the total displacement field was considered the sum of a regular part $\hat{\mathbf{u}}$ on Ω and a discontinuous part corresponding to the displacement jump $[\mathbf{u}]$, localized at the discontinuity surface Γ_d :

$$\mathbf{u}(\mathbf{x}) = \hat{\mathbf{u}}(\mathbf{x}) + \mathcal{H}_{\Gamma_d}[\mathbf{u}(\mathbf{x})], \quad (1)$$

where \mathcal{H}_{Γ_d} was defined as

$$\mathcal{H}_{\Gamma_d} = H_{\Gamma_d} - (1-r) \quad 0 \leq r \leq 1 \quad (2)$$

and H_{Γ_d} is the Heaviside function at the discontinuity Γ_d ,

$$H_{\Gamma_d} = \begin{cases} 1 & \text{if } \mathbf{x} \in \Omega^+ \\ 0 & \text{otherwise.} \end{cases} \quad (3)$$

Similar to the work presented in Lotfi and Shing (1995), the scalar parameter r defined how the jump

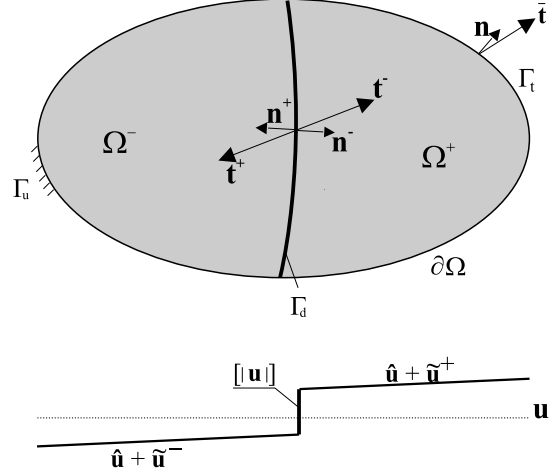


Figure 1: Domain Ω crossed by a discontinuity surface Γ_d

was transmitted to the domain Ω : if $r = 1$ the jump was fully transmitted from Ω^- to Ω^+ .

An alternative way is adopted here, where separate displacement fields are defined in Ω^+ and Ω^- :

$$\mathbf{u}(\mathbf{x}) = \begin{cases} \hat{\mathbf{u}}(\mathbf{x}) + \tilde{\mathbf{u}}^+(\mathbf{x}) & \text{if } \mathbf{x} \in \Omega^+ \\ \hat{\mathbf{u}}(\mathbf{x}) + \tilde{\mathbf{u}}^-(\mathbf{x}) & \text{if } \mathbf{x} \in \Omega^-. \end{cases} \quad (4)$$

In equation (4), $\tilde{\mathbf{u}}$ is the additional displacement field due to the discontinuity jump $[\mathbf{u}]$, such that:

$$[\mathbf{u}] = \tilde{\mathbf{u}}^+ - \tilde{\mathbf{u}}^- \quad \text{at } \Gamma_d \quad (5)$$

The regular strain field is obtained from the continuous part of the displacement field:

$$\hat{\boldsymbol{\varepsilon}} = \nabla^s \hat{\mathbf{u}} \quad \text{in } \Omega \setminus \Gamma_d \quad (6)$$

where $(\cdot)^s$ refers to the symmetric part of (\cdot) . The total strain in the body is given by:

$$\boldsymbol{\varepsilon} = \nabla^s \mathbf{u} = \nabla^s \hat{\mathbf{u}} + \tilde{\boldsymbol{\varepsilon}} \quad \text{in } \Omega \setminus \Gamma_d \quad (7)$$

$$\boldsymbol{\varepsilon} = \nabla^s \mathbf{u} = \underbrace{\nabla^s \hat{\mathbf{u}} + \tilde{\boldsymbol{\varepsilon}}}_{\text{bounded}} + \underbrace{\delta_{\Gamma_d}([\mathbf{u}] \otimes \mathbf{n})^s}_{\text{unbounded}} \quad \text{in } \Omega, \quad (8)$$

where

$$\tilde{\boldsymbol{\varepsilon}} = \begin{cases} \nabla^s \tilde{\mathbf{u}}^+(\mathbf{x}) & \text{if } \mathbf{x} \in \Omega^+ \\ \nabla^s \tilde{\mathbf{u}}^-(\mathbf{x}) & \text{if } \mathbf{x} \in \Omega^-. \end{cases} \quad (9)$$

In equations (7) and (8), \otimes denotes a dyadic product and δ_{Γ_d} is the Dirac-delta function along surface Γ_d . Both the displacement field and the strain field are continuous in Ω^- and Ω^+ , since the unbounded term in equation (8) vanishes in $\Omega \setminus \Gamma_d = \Omega^- \cup \Omega^+$.

3 VARIATIONAL FORMULATION

The governing field equations are imposed separately in $\Omega \setminus \Gamma_d$ and on Γ_d . Together with the boundary conditions, they can be expressed as:

$$\nabla \cdot \boldsymbol{\sigma} + \mathbf{b} = \mathbf{0} \quad \text{in} \quad \Omega \setminus \Gamma_d \quad (10)$$

$$\boldsymbol{\varepsilon} = \nabla^s \mathbf{u} \quad \text{in} \quad \Omega \setminus \Gamma_d \quad (11)$$

$$\boldsymbol{\sigma} = \boldsymbol{\sigma}(\boldsymbol{\varepsilon}) \quad \text{in} \quad \Omega \setminus \Gamma_d \quad (12)$$

$$\mathbf{u} = \bar{\mathbf{u}} \quad \text{at} \quad \Gamma_u \quad (13)$$

$$\boldsymbol{\sigma} \cdot \mathbf{n} = \bar{\mathbf{t}} \quad \text{at} \quad \Gamma_t \quad (14)$$

$$\boldsymbol{\sigma}^+ \cdot \mathbf{n}^+ = \mathbf{t}^+ \quad \text{at} \quad \Gamma_d \quad (15)$$

$$\boldsymbol{\sigma}^- \cdot \mathbf{n}^- = \mathbf{t}^- \quad \text{at} \quad \Gamma_d \quad (16)$$

$$\mathbf{t}^+ = -\mathbf{t}^- = \mathbf{t} \quad \text{at} \quad \Gamma_d \quad (17)$$

where \mathbf{b} are the body forces and $\bar{\mathbf{u}}$ and $\bar{\mathbf{t}}$ are the prescribed displacements and tractions at the boundary, respectively. Equations (15 and 16) enforce traction continuity across the discontinuity surface Γ_d , where the tractions are denoted by \mathbf{t} . As depicted in fig.1, $\mathbf{n}^+ = -\mathbf{n}^-$, is the outward normal of Ω^+ and $\mathbf{t}^+ = -\mathbf{t}^-$ denotes the traction vector acting on Ω^+ .

Similar to the discrete-interface approach, the adopted weak form corresponds to the principle of virtual work applied to a body crossed by a discontinuity (Malvern 1969; Alfaiate et al. 2003a; Alfaiate et al. 2003b); taking variations of the total displacements (5) and assuming that the essential boundary conditions are satisfied, it holds

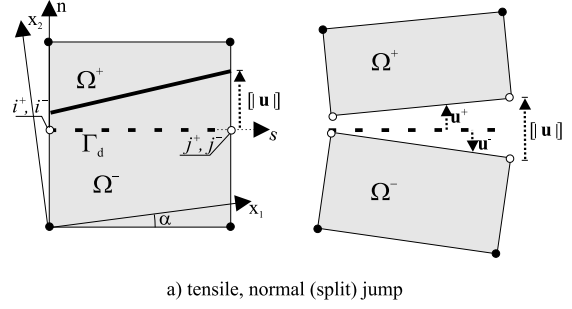
$$\begin{aligned} & - \int_{\Omega \setminus \Gamma_d} (\nabla^s \delta \mathbf{u}) : \boldsymbol{\sigma}(\hat{\boldsymbol{\varepsilon}}) d\Omega + \int_{\Omega \setminus \Gamma_d} \delta \mathbf{u} \cdot \mathbf{b} d\Omega \\ & + \int_{\Gamma_t} \delta \mathbf{u} \cdot \bar{\mathbf{t}} d\Gamma + \int_{\Gamma_d} (\delta \tilde{\mathbf{u}}^+ - \delta \tilde{\mathbf{u}}^-) \cdot \mathbf{t}^+ d\Gamma = 0, \end{aligned} \quad (18)$$

Taking in turn nonzero variations $\delta \tilde{\mathbf{u}}^+$, $\delta \tilde{\mathbf{u}}^-$ and $\delta \hat{\mathbf{u}}$, three variational statements are obtained:

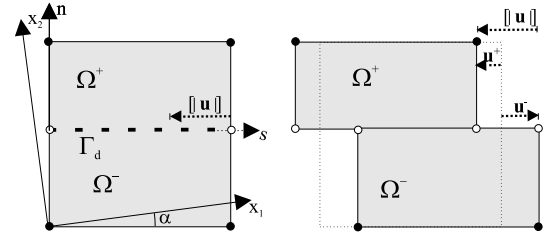
$$\begin{aligned} & - \int_{\Omega \setminus \Gamma_d} (\nabla^s \delta \hat{\mathbf{u}}) : \boldsymbol{\sigma}(\hat{\boldsymbol{\varepsilon}}) d\Omega + \int_{\Omega \setminus \Gamma_d} \delta \hat{\mathbf{u}} \cdot \mathbf{b} d\Omega \\ & + \int_{\Gamma_t} \delta \hat{\mathbf{u}} \cdot \bar{\mathbf{t}} d\Gamma = 0, \end{aligned} \quad (19)$$

$$\begin{aligned} & - \int_{\Omega^+} (\nabla^s \delta \tilde{\mathbf{u}}^+) : \boldsymbol{\sigma}(\hat{\boldsymbol{\varepsilon}}) d\Omega + \int_{\Omega^+} \delta \tilde{\mathbf{u}}^+ \cdot \mathbf{b} d\Omega \\ & + \int_{\Gamma_t^+} \delta \tilde{\mathbf{u}}^+ \cdot \bar{\mathbf{t}} d\Gamma + \int_{\Gamma_d} \delta \tilde{\mathbf{u}}^+ \cdot \mathbf{t}^+ d\Gamma = 0, \end{aligned} \quad (20)$$

$$\begin{aligned} & - \int_{\Omega^-} (\nabla^s \delta \tilde{\mathbf{u}}^-) : \boldsymbol{\sigma}(\hat{\boldsymbol{\varepsilon}}) d\Omega + \int_{\Omega^-} \delta \tilde{\mathbf{u}}^- \cdot \mathbf{b} d\Omega \\ & + \int_{\Gamma_t^-} \delta \tilde{\mathbf{u}}^- \cdot \bar{\mathbf{t}} d\Gamma - \int_{\Gamma_d} \delta \tilde{\mathbf{u}}^- \cdot \mathbf{t}^+ d\Gamma = 0, \end{aligned} \quad (21)$$



a) tensile, normal (split) jump



b) shear, tangential (slip) jump

Figure 2: Displacement jump in a four node element crossed by a discontinuity

Equation (19) is the usual principle of virtual work obtained for a continuum. The second and third variational statements in equations (20), (21) can be interpreted as the principle of virtual work applied to subdomains Ω^+ and Ω^- , respectively. As shown in Alfaiate et al. (2003b), this variational formulation is similar to the ones adopted in Lotfi and Shing (1995) and in the partition of unity method (Wells and Sluys 2001a), although, in the latter case, the jump is fully transmitted to Ω^+ ($\tilde{\mathbf{u}}^- = \mathbf{0}$).

4 FINITE ELEMENT APPROXIMATION

Consider a finite element discretisation of the 2D domain Ω . Assume that one element is crossed by a straight discontinuity Γ_d , which divides Ω in two sub-domains Ω^+ and Ω^- . A local frame (s, n) is introduced such that $s(\mathbf{x})$ is aligned with Γ_d and n is the normal to the discontinuity (fig. 2).

Recall equation (4). For the sake of simplicity, assume that the jump $[\mathbf{u}]$, $\tilde{\mathbf{u}}^+|_{\Gamma_d}$ and $\tilde{\mathbf{u}}^-|_{\Gamma_d}$ are linear functions of s , where

$$[\mathbf{u}] = [\mathbf{u}(s(\mathbf{x}))] = (\tilde{\mathbf{u}}^+ - \tilde{\mathbf{u}}^-)|_{\Gamma_d}. \quad (22)$$

In (fig.2), where $\hat{\mathbf{u}}$ is neglected for clarity, the total displacement field is depicted in two different situations: in (fig.2a) the discontinuity opens in the nor-

mal direction only, whereas in (fig.2b) the discontinuity represents a shear band undergoing sliding displacements.

If the jump is assumed to be constant across Γ_d , it is sufficient to adopt two internal nodes to represent the displacements $\tilde{\mathbf{u}}^+|_{\Gamma_d}$ and $\tilde{\mathbf{u}}^-|_{\Gamma_d}$. However, if higher order functions are considered to approximate the additional displacements $\tilde{\mathbf{u}}^\pm|_{\Gamma_d}$, more nodes are required, namely four nodes for a linear function, marked in white in fig.2, six nodes for a quadratic function and so forth. In the example above, the additional four nodes (i^+, i^- and j^+, j^- , each pair of nodes i and j initially coincide) are located at the intersection of Γ_d with the edges of the element.

In matrix form, for each finite element e with n nodes, the following approximation of the displacement field is adopted:

$$\begin{aligned} \hat{\mathbf{u}}^e &= \mathbf{N}^e(\mathbf{x})\hat{\mathbf{a}}^e && \text{in } \Omega^e \setminus \Gamma_d^e \\ [\mathbf{u}]^e &= \mathbf{N}_w^e[s(\mathbf{x})](\mathbf{w}^{e+} - \mathbf{w}^{e-}) && \text{at } \Gamma_d^e \end{aligned} \quad (23)$$

where \mathbf{N}^e contains the usual element shape functions, $\hat{\mathbf{a}}^e$ are the nodal degrees of freedom associated with $\hat{\mathbf{u}}^e$, \mathbf{N}_w^e are the shape functions used to approximate the jumps $[\mathbf{u}]^e$ and \mathbf{w}^{e+} and \mathbf{w}^{e-} are the degrees of freedom associated with $\tilde{\mathbf{u}}^{e+}|_{\Gamma_d^e}$ and $\tilde{\mathbf{u}}^{e-}|_{\Gamma_d^e}$, measured at nodes i^+, j^+ and i^-, j^- , respectively. If the number of node pairs in equations (23) used to approximate the jumps is n_w , \mathbf{N}_w^e is a $(2 \times 2n_w)$ matrix: if $n_w = 1$, \mathbf{N}_w^e is the unit matrix; if $n_w = 2$, \mathbf{N}_w^e contains linear shape functions, etc..

In most works adopting the embedded discontinuity approach, it was assumed that the total displacement field was approximated by the usual shape functions, so that the displacement jumps were *smear*d over the entire parent element (Simo et al. 1993; Wells and Sluys 2001b; Alfaiate et al. 2001; Alfaiate et al. 2003b). In the partition on unity method (Wells and Sluys 2001a), a *true* displacement jump is adopted at Γ_d^e , although the additional displacement field in Ω^{e+} is still obtained as $\tilde{\mathbf{u}}^{e+} = \mathbf{N}^e\mathbf{b}^e$, where \mathbf{b}^e are the additional degrees of freedom due to the displacement jump. Thus, in all these cases, the total strain field in $\Omega^e \setminus \Gamma_d^e$ is different from the regular strain field due to the continuum displacements, i.e.,

$$\boldsymbol{\varepsilon}^e \neq \hat{\boldsymbol{\varepsilon}}^e = \nabla^s \hat{\mathbf{u}}^e \text{ in } \Omega^e \setminus \Gamma_d^e \quad (24)$$

In Simo and Rifai (1990), it is assumed that S^h and $\tilde{\zeta}^h$ are L_2 orthogonal, where S^h and $\tilde{\zeta}^h$ are the admis-

sible stress space and the admissible enhanced strain space, respectively. As a result, the work done by the stresses on the enhanced strains in an element is null. Applying this orthogonality condition to Ω^{e+} and Ω^{e-} , gives

$$\int_{\Omega^{e+}} (\nabla^s \tilde{\mathbf{u}}^{e+})^T : \boldsymbol{\sigma}^e d\Omega = \int_{\Omega^{e-}} (\nabla^s \tilde{\mathbf{u}}^{e-})^T : \boldsymbol{\sigma}^e d\Omega = 0. \quad (25)$$

A physical interpretation of equation (25) can be given in the sense that the stresses in the element are only due to the regular part of the strain field, $\boldsymbol{\sigma} = \boldsymbol{\sigma}(\hat{\boldsymbol{\varepsilon}})$. This result, which was assumed in the variational formulation (see equations (18), (19), (20) and (21)) and in the works presented in Alfaiate et al. (2001), Alfaiate et al. (2003b), is also in agreement with the bounded nature of the stress field as stated by Oliver (1996). However, if inequality (24) holds, the orthogonality condition (25) is violated. In this work, equation (25) is enforced, by imposing that the displacements $\tilde{\mathbf{u}}^{e+}$ and $\tilde{\mathbf{u}}^{e-}$ induce a null enhanced strain field:

$$\begin{aligned} \tilde{\boldsymbol{\varepsilon}}^{e+} &= \nabla^s \tilde{\mathbf{u}}^{e+} = \mathbf{0} \text{ in } \Omega^{e+} \\ \tilde{\boldsymbol{\varepsilon}}^{e-} &= \nabla^s \tilde{\mathbf{u}}^{e-} = \mathbf{0} \text{ in } \Omega^{e-} \end{aligned} \quad (26)$$

Consequently, the additional displacement fields $\tilde{\mathbf{u}}^{e+}$ and $\tilde{\mathbf{u}}^{e-}$: i) must be evaluated separately in subdomains Ω^{e+} Ω^{e-} , respectively, and ii) correspond to rigid body motions:

$$\begin{aligned} \tilde{\mathbf{u}}^{e+} &= \mathbf{M}_w^e(\mathbf{x})\mathbf{w}^{e+} \text{ if } \mathbf{x} \in \Omega^{e+} \\ \tilde{\mathbf{u}}^{e-} &= \mathbf{M}_w^e(\mathbf{x})\mathbf{w}^{e-} \text{ if } \mathbf{x} \in \Omega^{e-}. \end{aligned} \quad (27)$$

In equations (27), \mathbf{M}_w^e is a $(2 \times 2n_w)$ matrix which generates rigid body motions of Ω^{e+} and Ω^{e-} . In the following, matrix \mathbf{M}_w^e is derived for linear functions \mathbf{w}^{e+} and \mathbf{w}^{e-} .

At any point \mathbf{x}^e , $\mathbf{x}^e \in \Omega^e$, the additional displacements $\tilde{\mathbf{u}}^{e\pm}$ are given by:

$$\tilde{\mathbf{u}}^{e\pm} = \begin{Bmatrix} -\tan \theta^\pm x_n + w_s^{j\pm} \\ \tan \theta^\pm x_s + w_n^{i\pm} \end{Bmatrix}. \quad (28)$$

In equation (28), θ^\pm is the rotation of $\Omega^{e\pm}$ relative to the s axis, such that:

$$\tan \theta^\pm = \frac{w_n^{j\pm} - w_n^{i\pm}}{l_d}, \quad (29)$$

x_s and x_n are the coordinates of \mathbf{x}^e in the local frame and $(w_s^{j\pm}, w_n^{j\pm})$, $(w_s^{i\pm}, w_n^{i\pm})$ are the components of

$\mathbf{w}^{e\pm}$ at node pairs i^\pm and j^\pm , respectively. Expressing the components of $\tilde{\mathbf{u}}^e$ and \mathbf{x}^e in the global frame (x_1, x_2) , leads to the definition of matrix \mathbf{M}_w^e , whose $(2 \times 2n_w)$ components read:

$$\mathbf{M}_w^{eT} = \begin{bmatrix} 1 - \frac{(x_2 - x_2^i) \sin \alpha}{l_d} & \frac{(x_1 - x_1^i) \sin \alpha}{l_d} \\ \frac{(x_2 - x_2^j) \cos \alpha}{l_d} & 1 - \frac{(x_1 - x_1^j) \cos \alpha}{l_d} \\ \frac{(x_2 - x_2^i) \sin \alpha}{l_d} & -\frac{(x_1 - x_1^i) \sin \alpha}{l_d} \\ -\frac{(x_2 - x_2^j) \cos \alpha}{l_d} & \frac{(x_1 - x_1^j) \cos \alpha}{l_d} \end{bmatrix}, \quad (30)$$

where l_d is the length of the discontinuity Γ_d^e and α is the angle between coordinates s and x_1 (see fig.2).

Finally, the displacement field in each element is given by:

$$\begin{aligned} \mathbf{u}^{e+} &= \mathbf{N}^e(\mathbf{x}) \hat{\mathbf{a}}^e + \mathbf{M}_w^e(\mathbf{x}) \mathbf{w}^{e+} & \text{if } \mathbf{x} \in \Omega^{e+} \\ \mathbf{u}^{e-} &= \mathbf{N}^e(\mathbf{x}) \hat{\mathbf{a}}^e + \mathbf{M}_w^e(\mathbf{x}) \mathbf{w}^{e-} & \text{if } \mathbf{x} \in \Omega^{e-} \\ [\mathbf{u}]^e &= \mathbf{N}_w^e[s(\mathbf{x})] (\mathbf{w}^{e+} - \mathbf{w}^{e-}) & \text{at } \Gamma_d^e. \end{aligned} \quad (31)$$

The regular strain field is approximated by:

$$\hat{\boldsymbol{\varepsilon}}^e = \mathbf{L} \mathbf{N}^e(\mathbf{x}) \hat{\mathbf{a}}^e = \mathbf{B}^e(\mathbf{x}) \hat{\mathbf{a}}^e, \quad (32)$$

where \mathbf{L} is the usual differential operator. Let the unknowns be \mathbf{a}^e , \mathbf{w}^{e+} and \mathbf{w}^{e-} , where \mathbf{a}^e are the total nodal displacements obtained at the regular nodes k , ($k \in \{1, 2, 3, 4\}$ in the example above):

$$\mathbf{a}^e = \hat{\mathbf{a}}^e + \tilde{\mathbf{a}}^e, \quad (33)$$

where

$$\begin{aligned} \tilde{\mathbf{a}}^{e+} &= \mathbf{M}_w^{ek+} \mathbf{w}^{e+} & \text{if } \mathbf{x} \in \Omega^{e+} \\ \tilde{\mathbf{a}}^{e-} &= \mathbf{M}_w^{ek-} \mathbf{w}^{e-} & \text{if } \mathbf{x} \in \Omega^{e-} \end{aligned} \quad (34)$$

and \mathbf{M}_w^{ek+} and \mathbf{M}_w^{ek-} correspond to matrix \mathbf{M}_w^e obtained at the k regular nodes in Ω^{e+} and Ω^{e-} , respectively. Equations (34) can be written in a more convenient way:

$$\tilde{\mathbf{a}}^e = \mathbf{M}_w^{ek+} \mathbf{w}^{e+} + \mathbf{M}_w^{ek-} \mathbf{w}^{e-} \quad (35)$$

since \mathbf{M}_w^{ek+} and \mathbf{M}_w^{ek-} can be expressed as

$$\begin{aligned} \mathbf{M}_w^{ek+} &= \mathbf{H}^+ \mathbf{M}_w^{ek} \\ \mathbf{M}_w^{ek-} &= \mathbf{H}^- \mathbf{M}_w^{ek}. \end{aligned} \quad (36)$$

In equations (36), \mathbf{H}^+ and \mathbf{H}^- are $(2n \times 2n)$ matrices: in \mathbf{H}^+ , only diagonal components related to

nodes in Ω^{e+} are equal to 1, whereas in \mathbf{H}^- , only diagonal components related to nodes in Ω^{e-} are equal to 1.

The regular strain field now reads:

$$\hat{\boldsymbol{\varepsilon}}^e = \mathbf{B}^e (\mathbf{a}^e - \mathbf{M}_w^{ek+} \mathbf{w}^{e+} - \mathbf{M}_w^{ek-} \mathbf{w}^{e-}). \quad (37)$$

The incremental stress field is

$$d\boldsymbol{\sigma}^e = \mathbf{D}^e \mathbf{B}^e (\mathbf{a}^e - \mathbf{M}_w^{ek+} \mathbf{w}^{e+} - \mathbf{M}_w^{ek-} \mathbf{w}^{e-}) \quad (38)$$

The tractions are obtained from the traction-jump law at the discontinuity. In incremental format this reads:

$$d\mathbf{t}^e = \mathbf{T}^e d[\mathbf{u}]^e = \mathbf{T}^e \mathbf{N}_w^e (d\mathbf{w}^{e+} - d\mathbf{w}^{e-}) \text{ at } \Gamma_d^e. \quad (39)$$

Discretising equations (19) to (21) by means of the field approximations given in equations (23), (38) and (39) gives

$$\mathbf{K}_{aa}^e d\hat{\mathbf{a}}^e = d\mathbf{f}_{ext}^e \quad (40)$$

$$\mathbf{K}_d d\mathbf{w}^{e+} = d\mathbf{f}_{w,ext}^{e+} \quad (41)$$

$$\mathbf{K}_d d\mathbf{w}^{e-} = d\mathbf{f}_{w,ext}^{e-} \quad (42)$$

where

$$d\hat{\mathbf{a}}^e = (d\mathbf{a}^e - \mathbf{M}_w^{ek+} d\mathbf{w}^{e+} - \mathbf{M}_w^{ek-} d\mathbf{w}^{e-}), \quad (43)$$

$$\mathbf{K}_{aa}^e = \int_{\Omega^e} \mathbf{B}^{eT} \mathbf{D}^e \mathbf{B}^e d\Omega, \quad (44)$$

$$\mathbf{K}_d^e = \int_{\Gamma_d^e} \mathbf{N}_w^{eT} \mathbf{T}^e \mathbf{N}_w^e d\Gamma, \quad (45)$$

and

$$d\mathbf{f}_{ext}^e = \int_{\Omega^e} \mathbf{N}^{eT} d\mathbf{b}^e d\Omega + \int_{\Gamma_f^e} \mathbf{N}^{eT} d\tilde{\mathbf{t}}^e d\Gamma, \quad (46)$$

$$d\mathbf{f}_{w,ext}^{e+} = \int_{\Omega^{e+}} \mathbf{M}_w^{ek+T} d\mathbf{b}^e d\Omega + \int_{\Gamma_r^+} \mathbf{M}_w^{ek+T} d\tilde{\mathbf{t}}^e d\Gamma, \quad (47)$$

$$d\mathbf{f}_{w,ext}^{e-} = \int_{\Omega^{e-}} \mathbf{M}_w^{ek-T} d\mathbf{b}^e d\Omega + \int_{\Gamma_r^-} \mathbf{M}_w^{ek-T} d\tilde{\mathbf{t}}^e d\Gamma. \quad (48)$$

Note that, in equations (41) and (42), the terms related to the gradient of the enhanced strain field are absent, since $\nabla^s \delta \tilde{\mathbf{u}}^e = \mathbf{0}$.

Similar to the works presented in Alfaiate et al. (2003a) and Alfaiate et al. (2003b), the additional nodes are global; thus, for $n_w \geq 2$ continuity of the jumps at the discontinuities across the element boundaries is automatically enforced.

Finally, it should be noted that, independently of the parent element chosen, for a straight discontinuity Γ_d^e the rigid body motions of Ω^{e+} and Ω^{e-} are totally defined by six independent degrees of freedom. In fact, it is imposed that (see fig.2b):

$$\begin{aligned} dw_s^{i+} &= dw_s^{j+} \\ dw_s^{i-} &= dw_s^{j-}. \end{aligned} \quad (49)$$

In previous embedded formulations presented in Alfaiate et al. (2003a) and Alfaiate et al. (2003b), the adopted additional degrees of freedom are the jumps \mathbf{w}^e , instead of the displacements \mathbf{w}^{e+} and \mathbf{w}^{e-} . However, as described in section 2, an additional scalar parameter r is also introduced, which enters the formulation if non-homogeneous jumps are considered in each element. In section 6, it will be shown that the choice of this parameter is not arbitrary. Furthermore, both formulations can be made equivalent. For this purpose, the number of degrees of freedom of the jump formulation must be set to six. As an example, consider the following degrees of freedom:

$$(w_n^i, w_s^i, w_n^j, r_n^i, r_s^i, r_n^j), \quad (50)$$

where i and j correspond to two additional nodes located at the edges of the parent element, r_n^i is the scalar parameter which defines how the normal jump component is transmitted to domains Ω^{e+} and Ω^{e-} at node i and r_s^i and r_n^j are defined similarly. This relationship between this formulation and the jump formulation will be further developed in the future.

Finally, the fact that only six additional independent degrees are needed to describe the kinematics of a straight discontinuity differs from the partition of unity method where, regardless of the parent element chosen, the number of the corresponding degrees of freedom is always doubled.

5 MATERIAL AND NUMERICAL MODELS

In this Section, the material and numerical models are described. A linear elastic bulk behaviour is adopted, whereas a localized damage model is used for the traction-jump law at the discontinuity. An isotropic traction-jump law is adopted (Alfaiate et al. 2001):

$$\mathbf{t} = (1 - d)\mathbf{T}_{el}\mathbf{w}, \quad (51)$$

where $0 \leq d \leq 1$ is a scalar damage variable and \mathbf{T}_{el} is the *elastic* constitutive tensor in which non-diagonal terms are zero and diagonal terms are

penalty functions used to prevent overlapping of crack faces under crack closure. The evolution of damage is given by:

$$d = d(\kappa) = 1 - \exp\left(-\frac{f_t}{G_F}\kappa\right), \quad (52)$$

where κ is a scalar variable taken equal to the maximum positive normal jump component:

$$\kappa = \max\langle w_n \rangle^+, \quad \kappa \geq 0, \quad \dot{\kappa} \geq 0, \quad (53)$$

f_t is the tensile strength and G_F is the fracture energy. A loading function is defined as

$$f = w_n - \kappa. \quad (54)$$

In this paper, only mode I opening is considered, i.e. discontinuities open perpendicularly to the direction of the maximum principal stress σ_I whenever

$$\sigma_I = f_t. \quad (55)$$

No shear tractions are allowed at the discontinuities during crack evolution. More general opening criteria will be considered in future works.

The embedding discontinuity technique as well as the fulfillment of the opening criterion were described in Alfaiate et al. (2003b), whereas crack path continuity is enforced according to an algorithm similar to the one presented in Alfaiate et al. (2001).

6 NUMERICAL EXAMPLES

Two examples are presented. The first example is a constant strain triangle, submitted to tension. Due to the asymmetry, the horizontal discontinuity, introduced at the centroid, opens at one of the edges only, as depicted in fig.3 where the deformed meshes obtained from the embedded discontinuity example and a discrete-interface test are presented. In this figure, the deformed mesh obtained in Alfaiate et al. (2003b) is also shown, where the displacements were *smeared* over the entire element. Nevertheless, the load-displacement curve still matches the other two rather well. In fig. 4, a perfect match between the load-displacement curves obtained with the two approaches is presented.

The second test is a double-cantilever beam, where a vertical discontinuity is prescribed in the middle of the specimen, both with the embedded

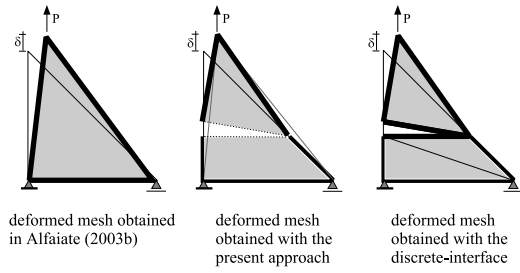


Figure 3: Asymmetric triangle submitted to tension

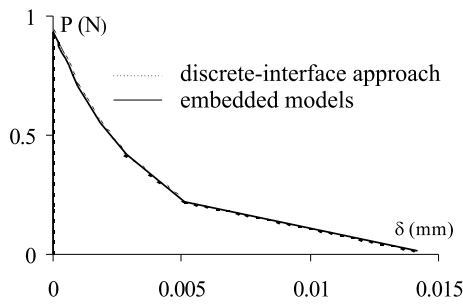


Figure 4: Load displacement curves corresponding to fig.3

formulation presented here and with the discrete-interface approach. In fig.5 the deformed meshes are presented and in fig.6 the load-displacement curves are shown. The response with the two techniques is again identical. In the latter figure, other results obtained with a previous formulation (Alfaiate et al. 2003a) are also shown. In this case, two values were adopted for the scalar parameter r defined in equation (2): $r = 0.5$ and $r = 1.0$. In the former case, it can be seen that the solution remains symmetric, whereas in the latter case, the solution is asymmetric, leading to a different load-displacement curve.

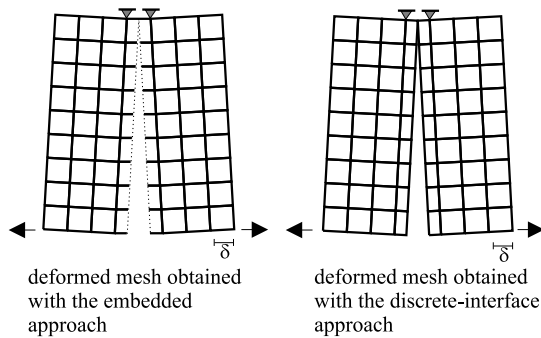


Figure 5: Double cantilever beam

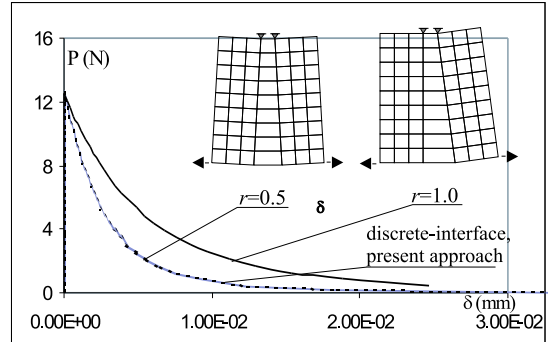


Figure 6: Double cantilever beam: load displacement curves

In fact, this is a particular case in which the boundary conditions do not contribute to eliminate the arbitrariness of parameter r . In general, the essential boundary conditions lead to a solution which does not depend significantly upon this scalar parameter. In the results presented in Alfaiate et al. (2003a) and Alfaiate et al. (2003b), r was taken equal to 0.5, although values of $r = 1.0$ were often used with similar results. In the latter case, the jump was fully transmitted to Ω^{e+} as assumed in the partition of unity formulation (Wells and Sluys 2001a). Note that, in the present formulation the solution is no longer arbitrary since the displacements induced by the jumps are evaluated separately in Ω^{e+} and Ω^{e-} .

7 CONCLUSIONS

In this paper, a *discrete strong embedded discontinuity approach (DSDA)* is proposed as an extension of previous strong embedded discontinuity formulations:

- i. similar to the discrete-interface approach, the element crossed by a discontinuity is divided into two subdomains;
- ii. however, no remeshing is necessary since these two subdomains are not considered as new elements;
- iii. instead, for each finite element, the variational formulation is split into three variational statements, similar to the work presented in Wells and Sluys (2001a);
- iv. the additional displacements due to the displacement jump at the discontinuity are considered rigid body motions in Ω^{e+} and Ω^{e-} ;

- v. due to this fact, it is shown that the orthogonality condition introduced in Simo and Rifai (1990) is fulfilled exactly on $\Omega^e \setminus \Gamma_d^e$;
- vi. moreover, only six additional degrees of freedom per parent element are necessary, as long as the discontinuity remains straight.

Finally, it should be emphasized that the strong embedded discontinuity formulation, either based on a discrete approach in this work, or derived from a continuum (Oliver et al. 2002), remains quite a general and powerful tool to model strain softening in a continuum.

Acknowledgements

I am most grateful to professor J. A. C. Martins from the Departement of Civil Engineering of the Instituto Superior Técnico, for the interesting discussions on this subject.

REFERENCES

- Alfaiate, J., Simone, A. & Sluys, L. J. 2003a. A new approach to strong embedded discontinuities. In N. Bicanic, R. de Borst, H. Mang, and G. Meschke (Eds.), *EURO-C 2003, Computational Modelling of Concrete Structures*, St. Johann im Pongau, Austria.
- Alfaiate, J., Simone A., & Sluys, L. J. 2003b. Non-homogeneous displacement jumps in strong embedded discontinuities. *International Journal of Solids and Structures* 40(21), 5799–5817.
- Alfaiate, J. & Sluys, L. J. 2002. Analysis of a compression test on concrete using strong embedded discontinuities. In H. Mang, F. Rammerstorfer, and J. Eberhardsteiner (Eds.), *WCCM V, Fifth World Congress on Computational Mechanics*, <http://wccm.tuwien.ac.at>, Vienna, Austria.
- Alfaiate, J., Wells, G. N., & Sluys, L. J. 2001. On the use of embedded discontinuity elements with crack path continuity for mode I and mixed mode fracture. *Engineering Fracture Mechanics* 69(6), 661–686.
- Lotfi, H. R. & Shing, P. B. 1995. Embedded representation of fracture in concrete with mixed finite elements. *International Journal for Numerical Methods in Engineering* 38(8), 1307–1325.
- Malvern, L. E. 1969. *Introduction to the Mechanics of a Continuous Medium*. New Jersey: Prentice-Hall International.
- Oliver, J. 1996. Modelling strong discontinuities in solid mechanics via strain softening constitutive equations. Part 1: Fundamentals. *International Journal for Numerical Methods in Engineering* 39(21), 3575–3600.
- Oliver, J., Huespe, A. E., Pulido, M. D. G., & Chaves, E. 2002. From continuum mechanics to fracture mechanics: the strong discontinuity approach. *Engineering Fracture Mechanics* 69, 113–136.
- Samaniego, E. 2003. *Contributions of the continuum modelling of strong discontinuities in two-dimensional solids*. Ph. D. thesis, Universitat Politècnica de Catalunya.
- Simo, J. C., Oliver, J., & Armero, F. 1993. An analysis of strong discontinuities induced by strain-softening in rate-independent inelastic solids. *Computational Mechanics* 12, 277–296.
- Simo, J. C. & Rifai, M. S. 1990. A class of mixed assumed strain methods and the method of incompatible modes. *International Journal for Numerical Methods in Engineering* 29(8), 1595–1638.
- Simone, A., Wells, G. N., & Sluys, L. J. 2003. From continuous to discontinuous failure in a gradient-enhanced continuum damage model. *Computer Methods in Applied Mechanics and Engineering* 192(41–42), 4581–4607.
- Sluys, L. J. 1998. Modelling of crack propagation with embedded discontinuity elements. In H. Mihashi and K. Rokugo (Eds.), *Fracture Mechanics of Concrete Structures - FRAMCOS3*, Gifu, Japan, pp. 843–860. AEDIFICATIO.
- Wells, G. N. & Sluys, L. J. 2001a. A new method for modelling cohesive cracks using finite elements. *International Journal for Numerical Methods in Engineering* 50(2), 2667–2682.
- Wells, G. N. & Sluys, L. J. 2001b. Three-dimensional embedded discontinuity model for brittle fracture. *International Journal of Solids and Structures* 38(5), 897–913.